An In-body Far Field Wireless Power Transfer Link Under Homogenous Tissue Assumption

Mahdi Salimitorkamani*, Burak Ferhat Ozcan*, Ahmet Bilir*, Mehmet Cakicioglu*, Sema Dumanli*
*Electrical and Electronics Engineering Dept., Bogazici University, Istanbul, Turkiye, sema.dumanli@bogazici.edu.tr

***Abstract*—This paper presents the design, simulation, and experimental validation of an in-body far-field wireless power transfer link. The link consists an electrically small, low-profile implanted Huygens Source Antenna (HSA) resonating at 1.8 GHz and a wide-band on-body slot antenna that operates between 0.7 GHz and 2 GHz. A Capacitively Loaded Loop (CLL), driven with an SMA port via an unbalanced microstrip feed network acts as the primary source of the Magnetic Dipole (H Moment). The bottom layer hosts a pair of symmetric Near-Field Resonant Parasitic elements that are coupled to the central CLL, generating the orthogonal Electric Dipole (E Moment) component. The final dimensions of the antenna are $0.072\lambda_0 \times 0.090\lambda_0 \times 0.015\lambda_0$. The HSA exhibits an efficiency of 0.18% confirming its suitability for power-efficient implant-to-surface communication and future integration into WPT systems. A channel transmission coefficient of -20.9 dB was achieved for an implant depth of 20 mm through phantom measurements.**

I. Introduction

The advancements in implantable medical devices have revolutionized modern healthcare, enabling continuous in vivo sensing, physiological monitoring, and therapeutics [1]–[3]. However, power remains an open challenge for their long-term functionality [4]. Therefore, research interest has grown in Wireless Power Transfer (WPT) technologies as a promising technology to deliver power to implants non-invasively [5].

WPT systems utilizing radio-frequency (RF) electromagnetic waves are typically categorized by the field region: near-field, midfield, or far-field [6]. According to this classification critical design parameters such as the coupling mechanism, suitable frequency bands, effective working distance are determined [7]. Another significant aspect to be considered in in-body WPT is the fact that human tissues are inherently lossy, heterogeneous, and frequency-dependent. This causes conventional WPT approaches to suffer from poor efficiency and potential safety risks [7]. The system design should maximize power transfer efficiency as well as considering electromagnetic exposure to ensure patient safety and regulatory compliance. To meet these requirements, a variety of solutions were developed in the literature, each offering different advantages and trade-offs.

Recent research demonstrated the use of high-permittivity encapsulations to electrically enlarge the aperture of miniature patch antennas and dipoles, improving their impedance matching and radiation efficiency [8]–[10]. In parallel, miniaturized magnetic loops and multi-coil systems for resonant WPT were widely explored to enhance power delivery to subcutaneous implants via inductive coupling [11]–[13]. However, these

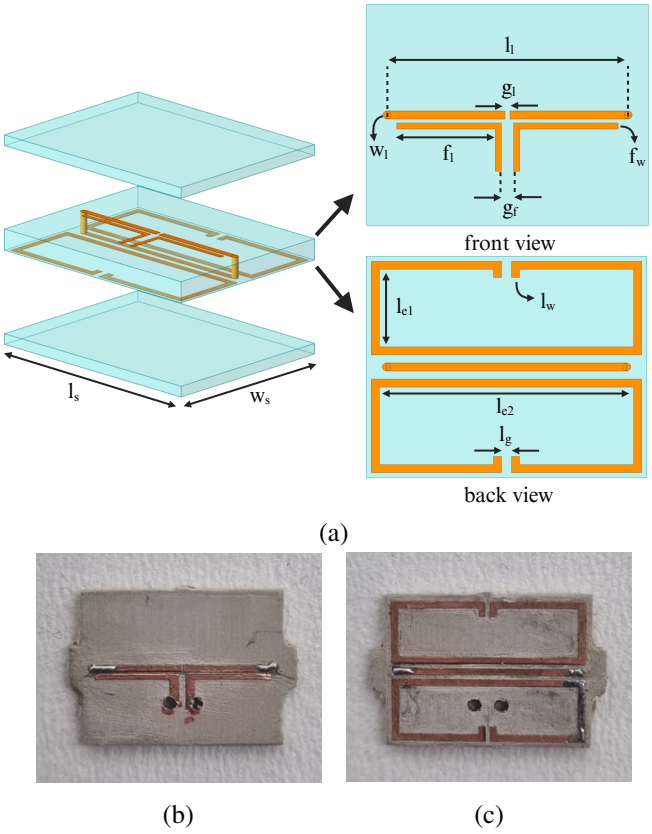

Fig. 1. (a) Geometry and configuration of the proposed HSA design. (b) Front and (c) back view of the fabricated HSA. Design parameters (all in mm) are given as: l_s = 14, w_s = 11, l_1 = 12, f_1 = 5.2, g_1 = 0.25, f_w = 0.3, g_f = 0.6, l_w = 0.8, l_{e1} = 3.85, l_{e2} = 12.7, l_g = 0.5.

approaches face inherent limitations. For example electric antennas often dissipate more energy in their near field compared to magnetic antennas. On the other hand, miniaturized loops suffer from low radiation resistance which limit their achievable efficiency [14]–[16]. This trade-off between antenna type, size, and near-field energy dissipation prompted further investigation. To address these limitations, the Huygens Source Antenna (HSA) emerged as a promising solution, engineered to produce a directional radiation pattern that focuses energy toward the external transmitter [17], [18].

In this study, we propose a far-field WPT system for in-body applications, comprising an implant HSA resonating at 1.8 GHz and an external on-body slot antenna operating from 0.7 to 2 GHz. The implant HSA is fabricated on a Rogers

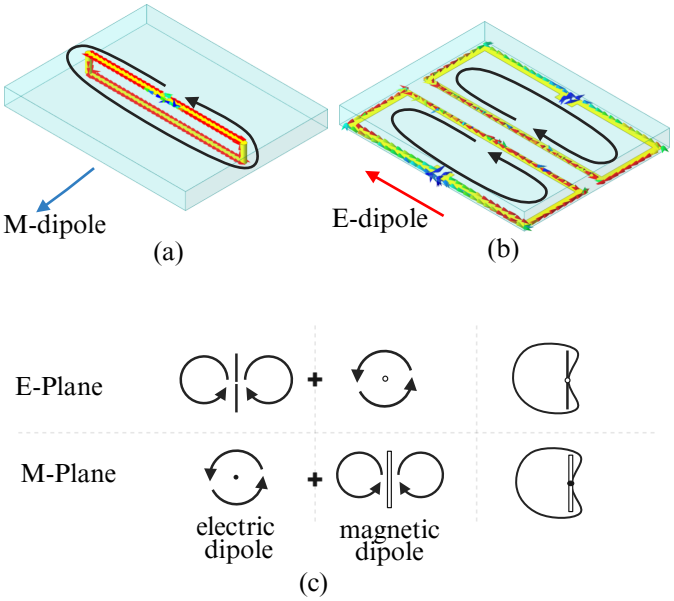

Fig. 2. (a) Generated magnetic dipole moment (**H**) by Capacitively Loaded Loop (CLL), (b) Generated electric dipole moment (**E**) , and (c) radiation mechanism of M and E dipole moment.

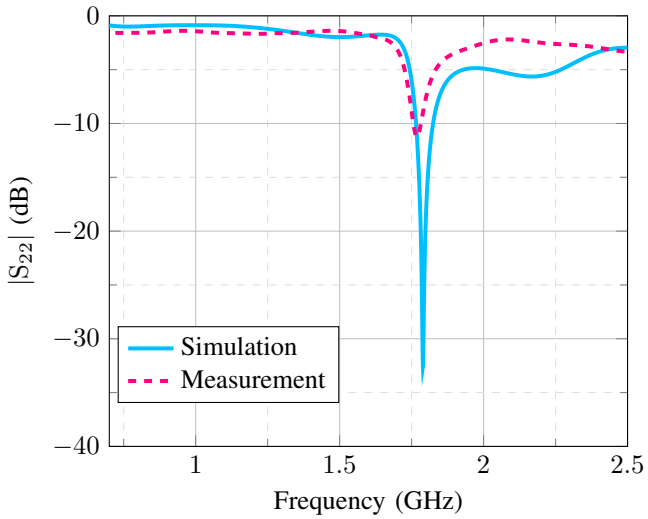

Fig. 3. Simulated and measured reflection coefficient $|S_{22}|$ of the HSA.

3010 substrate, encapsulated with a 0.64 mm thick Rogers 3010 layer. The operating frequency of 1.8 GHz is chosen for the target implantation depth of 25 mm to maximize far-field WPT efficiency for this depth, as established in [7]. The on-body slot antenna is designed to increase propagation into human body and compensate for frequency de-tuning that can occur in the implant antenna due to tissue variation.

The paper is structured as follows. Section II describes the design of the in-body HSA. Section III presents the design of the on-body slot antenna. The simulation and measurement analysis of the proposed system model are presented in Section IV. Finally, the conclusions are summarized in Section V.

II. In-body Huygens Source Antenna (HSA) Design

A HSA is designed on 1.27 mm thick Rogers 3010 with an effective permittivity of 10.2 and a loss tangent of 0.002 as seen Fig. 1. Furthermore, the antenna is sandwiched between two 0.64 mm thick Rogers 3010 layers and implanted in homogeneous muscle tissue phantom. This configuration of which design parameters are provided in the caption of Fig. 1 achieves a unidirectional radiation pattern.

The working principle of the proposed HSA is illustrated in Fig. 2. The primary radiator is a loop that is designed to function as a Capacitively Loaded Loop (CLL), generating the primary magnetic dipole moment (**H**) via circulating currents on it. **M** is quantified by the product of the circulating current (I_{loop}) and the loop's effective area (A): $\mathbf{M} = I_{loop}A$. Since the CLL is electrically small, A is approximated by its physical dimensions, with the length (L) being a key factor. Crucially, the presence of lossy tissue drastically alters the moment's magnitude and phase from its free-space value due to high dielectric loading. The high conductivity (σ) induces power loss, which attenuates the surface current density ($\mathbf{J}_s$) flowing along the loop, thus reducing the magnitude of I_{loop} and **M**. This reduction in **M** is the cause of the low efficiency in implanted systems. Its phase must be preserved at 90° relative to the parasitic **E**-dipole to maintain the unidirectional pattern required for efficient power transfer towards the external on-body antenna.

The orthogonal Electric Dipole (**E** Moment) is achieved parasitically by Near-Field Resonant Parasitic (NFRP) elements located on the bottom layer. The induced current distribution is presented in the Fig. 2(b). These parasitic elements are positioned to couple strongly with the **E** and **H** fields of the driven CLL. The induced currents in the NFRPs thus generate the necessary orthogonal **E**-field component. This electromagnetic synthesis fulfills the critical Huygens condition: the **E** and **H** dipoles are spatially co-located and exhibit the required 90° electrical phase difference, as conceptually derived from the radiation mechanism shown in Fig. 2(c) [19].

The reflection coefficient of the designed antenna is presented in Fig. 3. The simulations show a resonance at 1.8 GHz. A minor frequency shift to 1.78 GHz is observed in the measured response of the HSA prototype, which is attributed to fabrication tolerances.

III. On-body Slot antenna

The on-body element of the wireless power transfer system is a wideband on-body slot antenna with its design parameters are given in Fig. 4. The antenna is fabricated on a Rogers 3010 substrate and shown in Fig. 4 (a) and (b). The simulated and measured reflection coefficients $|S_{11}|$ are plotted in Fig. 5. The antenna achieves a wide operational bandwidth covering the 0.7 GHz to 2 GHz range. The wide band is critical for maintaining a link with the implanted device despite potential detuning due to tissue variation.

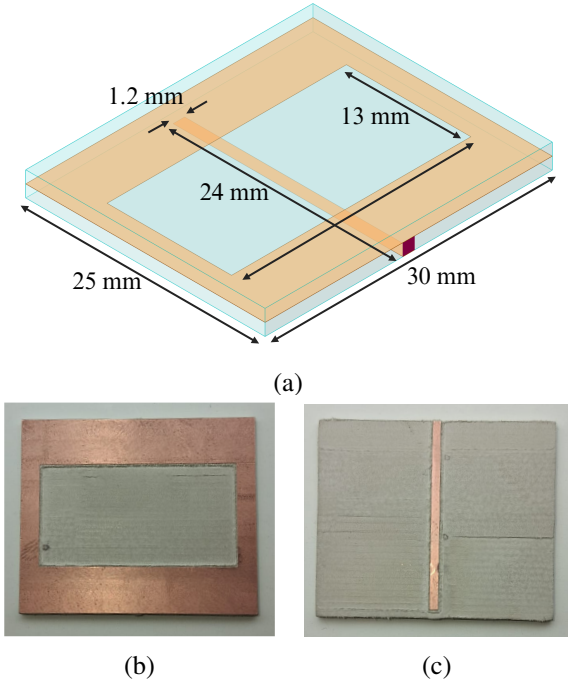

Fig. 4. (a) The geometry of the on-body slot antenna with a substrate thickness of 1.27 mm and a superstrate layer of 1.27 mm. (b) The front and (c) back view of the fabricated on-body slot antenna.

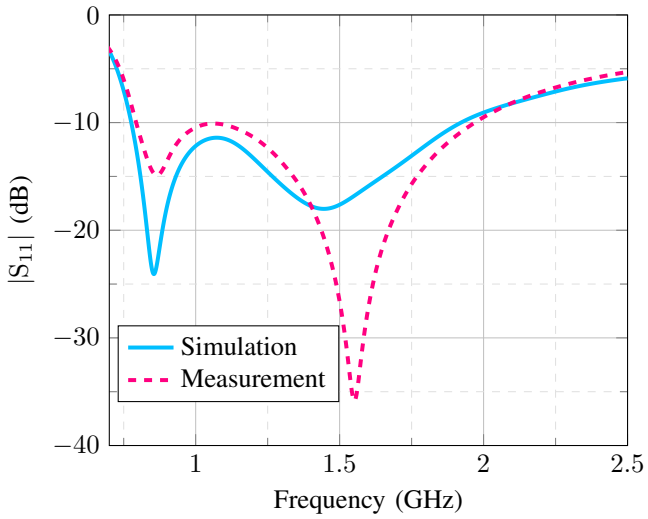

Fig. 5. Simulated and measured reflection coefficients $|S_{11}|$ of the on-body slot antenna.

IV. Simulation and Measurement Results

The electromagnetic performance of the wireless power transfer link is evaluated using a full-wave simulation environment and a measurement set-up including the implant and on-body antennas and muscle mimicking phantom.

The simulated model consists of a rectangular muscle tissue phantom with dimensions of 100 mm × 100 mm × 80 mm as seen in Fig. 6. The HSA is embedded within the muscle phantom at 25 mm depth, while the on-body slot antenna is

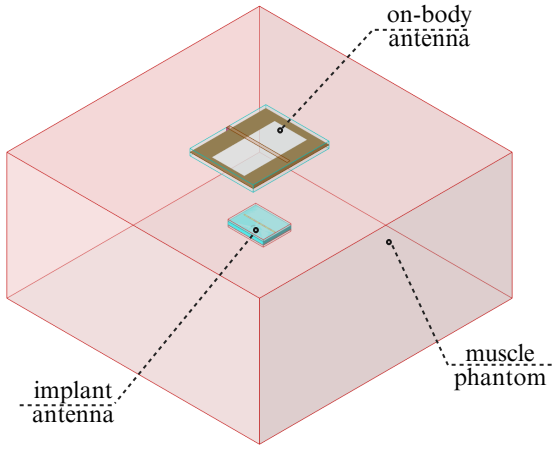

Fig. 6. Simulation model of the WPT system, showing the in-body HSA immersed in the tissue phantom and the on-body slot antenna.

positioned directly on its surface. The transmission coefficient $|S_{21}|$ is then simulated to quantitatively assess the power transfer efficiency.

To experimentally validate the simulated performance, the measurement setup shown in Fig. 7 is used. A rectangular container is fabricated with plexiglass and filled with a liquid muscle phantom prepared using Triton X-100 [20]. The phantom mimics the dielectric properties of muscle tissue at 1.8 GHz with a dielectric permittivity of 54.5 and conductivity of 1.34. Note that the corresponding values provided in IT'IS foundation are 53.5 and 1.34 respectively [21]. The cable connected to the implant antenna is encapsulated with a 3D printed tunnel and a ferrite ring is placed over the coaxial cable near the antenna feed point to suppress common-mode currents. The transmission coefficient between the implant antenna and the on-body antenna is measured for implant varying depths from 10 mm to 70 mm. The measured transmission coefficients and simulated transmission coefficient at 25 mm is plotted in Fig. 8. Good agreement between the simulation and measurements is observed especially at 1.8 GHz where the phantom is tuned. The transmission coefficient exceeds -45 dB even at 7 cm.

.

V. Conclusion

This paper presented and validated an in-body far-field power transfer link utilizing a electrically small HSA with a size of $0.072\lambda_0 \times 0.090\lambda_0 \times 0.015\lambda_0$ operating at 1.8 GHz. The HSA employs a driven CLL to generate the primary magnetic dipole moment ($\mathbf{H}$), which electromagnetically couples to NFRP elements to establish the orthogonal electric dipole moment ($\mathbf{E}$). An external on-body slot antenna operating from 0.7-2 GHz is designed to propagate into human body. Experimental validation in a tissue-mimicking environment confirmed a transmission coefficient of -21 dB at a 20 mm

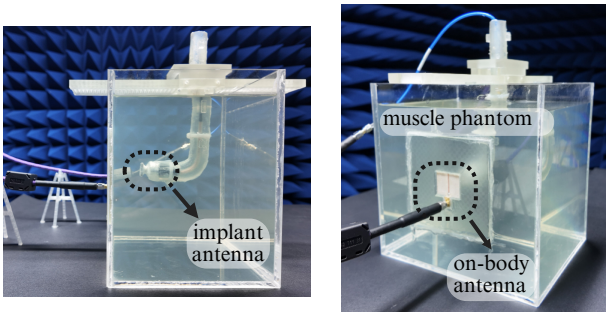

(a) (b)

Fig. 7. (a) Side view of the fabricated WPT setup showing the implant HSA, and (b) side view showing the muscle phantom and the on-body slot antenna.

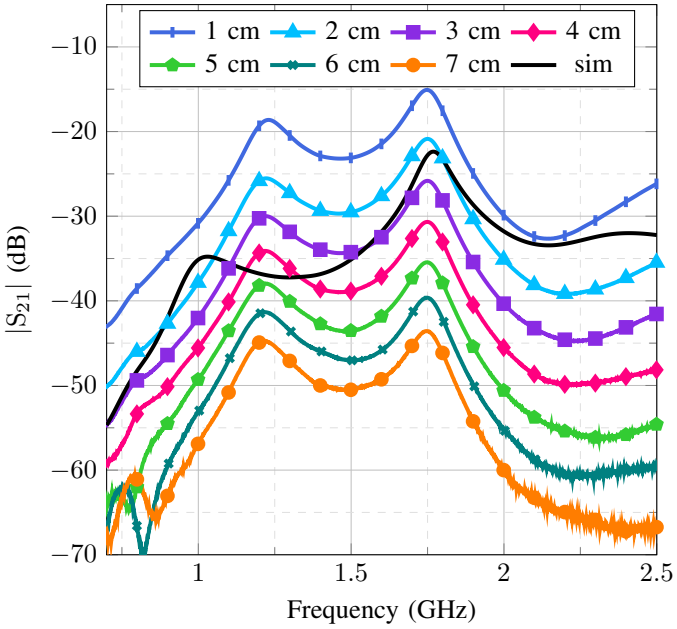

Fig. 8. The measured transmission coefficient $|S_{21}|$ across implant depths from 1 to 7 cm alongside the simulated result at a depth of 2.5 cm.

implant depth. Future work will integrate rectifying circuitry to realize a complete in-body WPT system.

References

[1] M. R. Yuce, "Implementation of wireless body area networks for healthcare systems," *Sensors and Actuators A: Physical*, vol. 162, no. 1, pp. 116–129, 2010.

[2] A. Abid, J. M. O'Brien, T. Bensel, C. Cleveland, L. Booth, B. R. Smith, R. Langer, and G. Traverso, "Wireless power transfer to millimeter-sized gastrointestinal electronics validated in a swine model," *Scientific reports*, vol. 7, no. 1, p. 46745, 2017.

[3] U. Anwar, Z. Liu, and D. Markovic, "A 6.78-mhz burst-mode controlled inductive wireless power transfer system for biomedical implants with back-channel communication eliminated using transmitter q-factor detection," *IEEE Journal of Emerging and Selected Topics in Power Electronics*, vol. 10, no. 5, pp. 6383–6395, 2022.

[4] W. Ouyang, W. Lu, Y. Zhang, Y. Liu, J. U. Kim, H. Shen, Y. Wu, H. Luan, K. Kilner, S. P. Lee *et al.*, "A wireless and battery-less implant for multimodal closed-loop neuromodulation in small animals," *Nature Biomedical Engineering*, vol. 7, no. 10, pp. 1252–1269, 2023.

[5] A. Iqbal, M. Al-Hasan, I. B. Mabrouk, A. Basir, M. Nedil, and H. Yoo, "Biotelemetry and wireless powering of biomedical implants using a rectifier integrated self-diplexing implantable antenna," *IEEE Transactions on Microwave Theory and Techniques*, vol. 69, no. 7, pp. 3438–3451, 2021.

[6] T. Sun, X. Xie, and Z. Wang, *Wireless power transfer for medical microsystems*. Springer, 2013.

[7] Í. Soares, Z. Šipuš, A. Skrivervik, R. Sauleau, A. Alù, J. Ho, and D. Nikolayev, "Wireless powering for long-lasting deep-body bioelectronic devices: Solutions, limitations, and new technologies [bioelectromagnetics]," *IEEE Antennas and Propagation Magazine*, vol. 67, no. 3, pp. 74–86, 2025.

[8] A. Basir and H. Yoo, "Efficient wireless power transfer system with a miniaturized quad-band implantable antenna that deep-body multitasking implants," *IEEE Transactions on Microwave Theory and Techniques*, vol. 10, no. 5, pp. 1843–1853, 2020.

[9] D. Nikolayev, A. K. Skrivervik, J. S. Ho, M. Zhadobov, and R. Sauleau, "Reconfigurable dual-band capsule-conformal antenna array for in-body bioelectronics," *IEEE Transactions on Antennas and Propagation*, vol. 70, no. 5, pp. 3749–3761, 2022.

[10] D. Nikolayev, W. Joseph, A. Skrivervik, M. Zhadobov, L. Martens, and R. Sauleau, "Dielectric-loaded conformal microstrip antennas for versatile in-body applications," *IEEE Antennas and Wireless Propagation Letters*, vol. 18, no. 12, pp. 2686–2690, 2019.

[11] J. Wang *et al.*, "A 403 mhz wireless power transfer system with tuned split-ring loops for implantable medical devices," *IEEE Transactions on Antennas and Propagation*, vol. 10, no. 2, pp. 1355–1366, 2022.

[12] Y. Jia, S. A. Mirbozorgi, P. Zhang, O. T. Inan, W. Li, and M. Ghovanloo, "A dual-band wireless power transmission system for evaluating mm-sized implants," *IEEE Transactions on Biomedical Circuits and Systems*, vol. 13, no. 4, pp. 595–607, 2019.

[13] M. Schormans, V. Valente, and A. Demosthenous, "Practical inductive link design for biomedical wireless power transfer: A tutorial," *IEEE Transactions on Biomedical Circuits and Systems*, vol. 12, no. 5, pp. 1112–1130, 2018.

[14] I. V. Soares *et al.*, "Wireless powering efficiency of deep-body implantable devices," *IEEE Transactions on Microwave Theory and Techniques*, vol. 71, no. 6, pp. 2680–2692, 2023.

[15] A. K. Skrivervik, M. Bosiljevac, and Z. Sipus, "Fundamental limits for implanted antennas: Maximum power density reaching free space," *IEEE Transactions on Antennas and Propagation*, vol. 67, no. 8, pp. 4978–4988, 2019.

[16] J. Liska, M. Gao, L. Jelinek, E. R. Algarp, A. K. Skrivervik, and M. Capek, "Maximum radiation efficiency of arbitrarily shaped implantable antennas," *IEEE Transactions on Antennas and Propagation*, vol. 72, no. 4, pp. 3507–3516, 2024.

[17] P. Jin and R. W. Ziolkowski, "Metamaterial-inspired, electrically small huygens sources," *IEEE Antennas and Wireless Propagation Letters*, vol. 9, pp. 501–505, 2010.

[18] W. Lin, R. W. Ziolkowski, and J. Huang, "Electrically small, low-profile, highly efficient, huygens dipole rectennas for wirelessly powering internet-of-things devices," *IEEE Transactions on Antennas and Propagation*, vol. 67, no. 6, pp. 3670–3679, 2019.

[19] L. Matekovits, B. K. Kanaujia, J. Kishor, and S. K. Gupta, *Printed Antennas for 5G Networks*. Springer, 2022.

[20] S. Romeo, L. D. Donato, O. M. Bucci, I. Catapano, L. Crocco, M. R. Scarfì, and R. Massa, "Dielectric characterization study of liquid-based materials for mimicking breast tissues," *Microwave and Optical Technology Letters*, vol. 53, pp. 1276–1280, 2011.

[21] IT'IS Foundation. (2025) IT'IS Database for Thermal and Electromagnetic Parameters of Biological Tissues. [Accessed: 20-Oct-2025]. [Online]. Available: https://itis.swiss/virtual-population/tissue-properties/database/dielectricproperties